3D bioprinting of biomimetic alginate/gelatin/chondroitin sulfate hydrogel nanocomposites for intrinsically chondrogenic differentiation of human mesenchymal stem cells

Felipe Olate-Moya[a, b],* Gerard Rubí-Sans[d, e], Elisabeth Engel[c, d, e], Miguel Ángel Mateos-Timoneda[f, g] and Humberto Palza[a, b] *

[a] Departamento de Ingeniería Química, Biotecnología y Materiales, Facultad de Ciencias Físicas y Matemáticas, Universidad de Chile, Avenida Beauchef 851, 8370458 Santiago, Chile.

[b] IMPACT, Center of Interventional Medicine for Precision and Advanced Cellular Therapy, Avenida Monseñor Álvaro del Portillo 12455, 7620086 Las Condes, Chile.

[c] IMEM-BRT Group, Departament de Ciència i Enginyeria de Materials, EEBE, Universitat Politècnica de Catalunya (UPC), C/Eduard Maristany 10-14, 08019 Barcelona, Spain

[d] Institute for Bioengineering of Catalonia (IBEC), The Barcelona Institute of Science and Technology (BIST), Carrer de Baldiri Reixac, 10, 12, 08028, 08019 Barcelona, Spain.

[e] CIBER en Bioingeniería, Biomateriales y Nanomedicina, CIBER-BBN, 50018 Zaragoza, Spain

[f] Bioengineering Institute of Technology, Universitat Internacional de Catalunya, Josep Trueta Street s/n, 08195, Sant Cugat del Vallès (Barcelona), Spain.

[g] Department of Basic Sciences, Faculty of Medicine and Health Sciences, Univesitat Internacional de Catalunya, Josep Trueta Street s/n, 08195, Sant Cugat del Vallès (Barcelona), Spain.

* Corresponding authors:

E-mail: felipe.olate@ing.uchile.cl (F. Olate-Moya); hpalza@ing.uchile.cl (H. Palza)

Abstract

3D-printed hydrogel scaffolds biomimicking the extracellular matrix (ECM) are key in cartilage tissue engineering (CTE) as they can enhance the chondrogenic differentiation of mesenchymal stem cells (MSCs) through the presence of active nanoparticles, such as graphene oxide (GO). Here, biomimetic hydrogels were developed by crosslinking alginate, gelatin, and chondroitin sulfate biopolymers in the presence of GO as a bioactive filler, with excellent processability for developing bioactive 3D printed scaffolds and for the bioprinting process. A novel bioink based on our hydrogel with embedded human MSCs presented a cell survival rate near 100 % after the 3D bioprinting process. The effect of processing and filler concentration on cell differentiation was further quantitatively evaluated. The nanocomposited hydrogels render high MSCs proliferation and viability, exhibiting intrinsic chondroinductive capacity without any exogenous factor when used to print scaffolds or to bioprint constructs. The bioactivity depended on the GO concentration, with the best performance at 0.1 mg mL^{-1}. These results were explained by the rational combination of the three biopolymers with GO nanoparticles having carboxylate and sulfate groups in their structures, therefore biomimicking the highly negatively charged ECM of cartilage. The bioactivity of this biomaterial and its good processability for 3D printing scaffolds and 3D bioprinting techniques open up a new approach to developing novel biomimetic materials for cartilage repair.

Keywords: Hydrogel composites, 3D printing, Tissue engineering.

1. Introduction

Bioactive hydrogels that mimic the extracellular matrix (ECM) have a key role in advanced regenerative medicine applications, especially in cartilage tissue engineering (CTE), for their potential in cartilage-associated disease treatment.[1–3] However, the effective clinical treatment of some relevant degenerative cartilage diseases, such as osteoarthritis, where the ECM of articular joints has progressively deteriorated, remains elusive.[4] In vitro and in vivo studies have evidenced that using mesenchymal stem cells (MSCs) in combination with bioactive and biomimetic hydrogels produces a synergistic effect on chondrogenesis and

neocartilage ECM production.[3] From the material point of view, cartilage ECM is mainly composed of type II collagen (COLL II), aggrecan (ACAN), and water.[3,5] The high content of collagen in animal tissues, besides the high availability of sources, bioactivity, low antigenicity, and cost-effectiveness, has motivated the use of hydrogels based on the collagen-derived gelatin macromolecule (GEL). This biopolymer is a water-soluble polypeptide obtained from the hydrolysis of insoluble collagen, the most abundant animal protein.[6] In particular, methacryloyl-modified GEL (GEL-MA) has been extensively used in tissue engineering, including CTE.[3,7] The photo-crosslinkable ability of GEL-MA allows the obtention of mechanically tunable and bioconjugate scaffolds exhibiting excellent cell adhesion and proliferation because of the arginyl-glycyl-aspartic acid (RGD) motifs in the polypeptide structure of GEL that interact with the integrin proteins of the cell membrane.[3,8] GEL has been further combined with glycosaminoglycans (GAGs), a family of negatively charged polysaccharide compounds, to develop biomimetic materials for CTE.[6] In particular, chondroitin sulfate (CS) is highlighted as a group of sulfated GAGs where the number and position of sulfate groups in the monomer structure define the type of classification (O, A, C, D, and E).[9] In the cartilage ECM, CS chains are bonded to aggrecan glycoprotein, which acts as a hydrogel that retains water molecules.[3,9] Aggrecan has a pivotal role in articular cartilage, such as compressive load bearing, protein linker, chondrocyte-chondrocyte and chondrocyte-ECM interactions, and tissue remodeling.[10] Particularly, CS-linked aggrecan proteoglycan modulates cell signaling pathways related to growth factors secretion, hedgehog and wingless-related proteins, and the initial stages of chondrogenesis in cartilage tissue.[11] Several investigations focused on biomimetic hydrogels using CS combined with proteins such as collagen or GEL to improve their processability and bioactivity.[12,13] For instance, photocrosslinking of methacryloyl-modified GEL and CS has been reported as cartilage ECM mimicking biomaterial.[14] This hydrogel upregulated the expression of chondrogenic COLL II-, SOX 9-, and ACAN-associated genes. Costantini et al. reported a bioink using bone marrow-derived MSCs (BM-MSCs) in combination with a mix of photo-crosslinked natural polymers (with vinyl moieties) such as alginate (ALG), GEL, CS, and hyaluronic acid (HA) as an ECM-mimetic platform in chondrogenic medium for CTE.[2] In another chemical biomimetic strategy, glutaraldehyde-crosslinked GEL-CS

nanofibrous scaffolds, evidence of improved chondrogenesis of human bone marrow-derived MSCs (hBM-MSCs) was found.[15] The electrospun scaffolds showed that increasing the CS content could increment the chondroinductivity of the biomaterial. In a recent study, CS was chemically modified with catechol groups (CS-CA) to enhance the in vitro chondrogenesis using human adipose-derived MSCs (hADMSCs) in a chondroinductive culture medium.[16] In vivo tests showed that this biomaterial induces neo-cartilage formation in a rabbit model. Soft hydrogels usually have been incorporated into a 3D-printed framework of biodegradable polymer mesh, such as polycaprolactone (PCL), to achieve suitable mechanical performance for CTE.[16,17] The above examples show that biomaterials chemically bonded to CS improve their performance in chondrogenesis. However, most of the research on CTE usually employs a biochemical cocktail of biomolecules, drugs, and growth factors to stimulate and improve the chondrogenic differentiation of MSCs, complementing the role of the biomimetic hydrogel itself.[18] However, these external compounds can present some issues related to their adverse side effects. For instance, transforming growth factor beta (TGF-β), the principal cytokine that induces chondrogenesis on MSCs,[18] can generate hypertrophic maturation, mineralization, secretion of inflammatory/angiogenic factors, and promotion of cancer progression and metastasis.[19,20] In this context, the design of intrinsical chondroinductive biomaterials for cartilage-associated disease treatment has been explored during the last few years.[21–23]

Intrinsically chondroinductive biomaterials are bioactive substances that might differentiate MSCs toward the chondrocyte phenotype without needing a culture medium supplemented with chondrogenic agents (e.g., TGF-β, dexamethasone, L-ascorbic acid, insulin-transferrin-selenium (ITS), and L-proline). Scaffolds based on decellularized cartilage could be considered a rational strategy to obtain intrinsically chondroinductive biomaterials, although they present some disadvantages, such as immunogenicity and low processability.[22] A more proper rational strategy for designing biomaterials with intrinsical and targeted MSCs differentiation is extending the biomimetic approach to replicate the chemical structure of the ECM that can induce MSCs to differentiate in the phenotypes of the specific tissue cells.[5]. This approach has been

widely studied using bone-mimetic components such as hydroxyapatite, tricalcium phosphate, and collagen for developing intrinsically osteoinductive biomaterials.[24] Intrinsically chondroinductive materials have been less studied, and they are mainly based on peptides with amino acid sequences derived from growth factors such as TGF-β and bone morphogenetic proteins (BMP).[21] In this regard, biopolymers already present in the ECM of cartilage, such as HA and CS, can also be chondroinductors on MSCs.[3]. Among the few intrinsically chondroinductive biomaterials, PCL with CS-modified surface, GEL-CS/PCL nanofibrous, macroporous GEL/HA/CS cryogels, and nanofibrous GEL/polyvinyl alcohol (PVOH)/CS scaffolds have been reported.[25–28] These examples prove that using CS as a biomaterial is a rational strategy to induce chondrogenesis intrinsically without exogen agents. The fundamental chondrogenic mechanism of CS is yet unknown; however, it may include direct cell-GAG interaction or CS binding to secreted growth factors, modulating the gene expression during the chondrocyte differentiation.[12]

One of the methodologies that have been gaining ground in the last decade in CTE is 3D printing, allowing the manufacture of scaffolds with complex tailor-made structures according to the patient's needs and the ability to control structural aspects such as pore size and chemical composition.[29] This methodology allows the next step in constructing biomimetic, functional, and heterogeneous structures (such as complex tissues and organs), manufacturing biologically functional constructs with embedded living cells in a hydrogel that replicates the native ECM through a process named 3D bioprinting. The basis of fabricating "living" 3D structures (biofabrication) is the formulation of a bioink composed of cells embedded in a hydrogel matrix.[30] In this context, bioinks composed of alginate (ALG) have been developed because of their advantage of rapid ionotropic gelation and cell cytocompatibility.[30–33] ALG is an anionic polysaccharide that, in solution, presents a transition from a viscous fluid to a rigid hydrogel through strong electrostatic interactions between divalent metal cations (e.g., calcium) and the α-L-guluronate segments present in the ALG chains. This feature is exploited in 3D printing/bioprinting to maintain the shape fidelity of the designed structure.[2] However, because this biopolymer comes mainly from marine algae, the interaction between ALG and

animal cells is rather low.[33] Therefore, for CTE applications, it is necessary to bioconjugate the ALG to impart bioactivity and thus enhance, for example, cell adhesion, proliferation, and differentiation.[6]

Despite the outstanding qualities of hydrogels as a material mimicking ECM, poor mechanical and processing properties remain a limitation for manufacturing 3D-printed hydrogel scaffolds for CTE applications.[3,15] There are several strategies to improve the mechanical properties of hydrogels, one of which is to crosslink the polymer chains covalently. This strategy is key in hydrogels' 3D printing/bioprinting, where even dual-stage crosslinking can be carried out.[2,34] Another widely used strategy is incorporating particles such as carbon-based nanomaterials as reinforcement of hydrogels.[35,36] Nanocomposited hydrogels further exhibit other properties such as optical activity, anisotropy, bioactivity, and rheology modulation of 3D printing inks.[32] These nanocomposited hydrogels are multifunctional biomaterials, and this versatility offers an integral alternative for CTE. One of the most interesting nanomaterials for CTE applications is graphene oxide (GO), a graphite-derived nanoparticle based on a single layer or few layers of carbon atoms with an aromatic structure (sp^2 hybridization) partially functionalized with groups rich in oxygen atoms (mainly carboxylate, hydroxyl, and epoxide groups).[36] GO is a water-dispersible nanoparticle that allows the formulation of reinforced hydrogel inks or bioinks. Incorporating GO into hydrogels can improve the mechanical properties of scaffolds or constructs and improve the rheological properties of inks/bioinks, resulting in better printability.[36,37] From a biological point of view, GO has also been shown to act as a carrier of bioactive molecules and promote the proliferation, alignment, and differentiation of MSCs.[35–38] 3D bioprinted constructs based on GO-doped GEL-MA/polyethylene glycol diacrylate (PEG-DA) hydrogel have been shown to promote chondrogenic differentiation of BM-MSCs in a chondrogenic medium.[39] The formulation with 0.1 mg mL^{-1} of GO into GEL-MA/PEG-DA bioink showed optimal cell proliferation and higher chondrogenic gene expression than hydrogel without GO. Our previous research demonstrated that GO in a biomimetic hydrogel further allowed the alignment of supported cells along the 3D printed filament direction (through liquid/crystal transition of the nanoparticle) and improved proliferation and differentiation.[23] This hydrogel based on ALG-CS-GEL (ACG) composited with GO (ACG/GO) showed an

intrinsic chondroinductivity, but the elucidation of the influence of biomaterial composition on chondrogenesis remains unknown.

Continuing our previous work using an ACG/GO hydrogel matrix that mimics the ECM of cartilage, where GO nanoparticles improve the printability and bioactivity of the material, this contribution explores the effect of CS, GO, and the biomaterial processing (testing either 3D printed scaffolds or bioprinting process) on the chondroinductivity of the biomimetic hydrogel by real-time quantitative reverse transcriptase-polymerase chain reaction (qRT-PCR). For this, hADMSCs were employed to evaluate the biological performance of the developed biomaterial. A novel bioink of hADMSCs embedded into a matrix based on the ACG/GO hydrogel was formulated, which showed high cytocompatibility and intrinsic chondroinductivity. The alginate present in the bioink allows better processability during bioprinting and provides a density of negative charges characteristic of the ECM of cartilage. Alginate was bioconjugated with gelatin (homologous to cartilage's collagen) and chondroitin sulfate (GAG present in the ECM of cartilage), biomimicking the native environment of the cartilage tissue. The nanoparticles of graphene oxide in the composite hydrogel provide a density of negative charges, improve printing quality, and promote chondrogenesis. These features offer a rationally designed biomaterial able to induce stem cell differentiation without the need for exogenous factors (such as TGF-β) or drugs for 3D bioprinting cartilage tissue engineering.

2. Materials and methods

2.1. Materials

The natural polymers alginic acid sodium salt from brown algae (ALG, M/G ratio = 0.72, Lot #BCBS1047V, Code 71238-250G), type A chondroitin sulfate sodium salt from the bovine trachea (CS, 85 % type A CS, and 15 % type C CS, Lot #SLBQ0017V, Code C9819-5G), and type A gelatin from porcine skin (GEL, gel strength 300, Lot #SLBQ9498V, Code G1890-100G) BioReagent grades were purchased from Sigma-Aldrich (Norway, China, and USA, respectively) and used as received. N-(3-dimethylaminopropyl)-N'-ethylcarbodiimide hydrochloride (EDC, Code 03449-5G), N-hydroxysuccinimide (NHS, Code 130672-5G), 2-(N-

morpholino)ethanesulfonic acid (MES, Code M3671-50G), methacrylic anhydride (MAA, Code 276685-100ML), graphite (fine powder extra pure, Code 1042062500), potassium permanganate (Code 1050821000), sodium nitrate (Code 1065371000), calcium chloride (Code 1023820500), sulfuric acid (Code 1018332500), hydrogen peroxide (Code 1072091000), ethanol (Code 1009832500), and deuterium oxide (Code 1133660025) were purchased from Sigma-Aldrich or Merck Millipore. 2-Aminoethyl methacrylate hydrochloride (AEMA, Code sc-254152) and 2-hydroxy-4'-(2-hydroxyethoxy)-2-methylpropiophenone photoinitiator (PI, Code sc-488409) were purchased from Santa Cruz Biotechnology (USA). Dialysis tube Spectra/Por 1 (MWCO = 6−8 kDa, 50 mm flat width, Code 132665) utilized in the purification of methacrylated biopolymers was purchased from Spectrum Laboratories. Type I (ultrapure) water was used for synthesis and purification.

2.2. Methods

2.2.1. Inks and bioink formulations

The natural polymers were functionalized with polymerizable methacryloyl groups to obtain ALG-MA, CS-MA, and GEL-MA, following previously reported methods.[40] ALG-MA was obtained by dissolution of 1 g of ALG in a buffer solution of MES 50 mM (pH=6.5) and NaCl 0.5 M. The carboxylic acid groups were activated by adding 0.87 g (4.6 mmol) of EDC and 0.26 g (2.3 mmol) of NHS. After 5 minutes of activation, 0.38 g (2.3 mmol) of AEMA was added to the mixture, which was then allowed to react for 24 hours at room temperature. The resulting methacrylated polymer was precipitated in absolute ethanol, separated by vacuum filtration, and dried in a vacuum oven at 60°C overnight. The dry product was dissolved in deionized water and dialyzed in a Spectra/Por 1 tube against deionized water for four days, with the dialysate water being changed every 12 hours. The purified product was then lyophilized using a Martin Christ Alpha 1-2 LDplus freeze-dryer and stored at −20 °C until further use. Similarly, the CS-MA was synthesized by dissolving 1 g of CS in a buffer solution of MES 50 mM (pH=6.5) and NaCl 0.5 M. After dissolving the biopolymer, 0.87 g (4.6 mmol) of EDC and 0.26 g (2.3 mmol) of NHS were added to the solution. After 5

minutes of reaction, 0.38 g (2.3 mmol) of AEMA was added to the mixture, which was then allowed to react for 24 hours at room temperature. CS-MA was purified by precipitation and dialysis, lyophilized, and stored at -20 °C following the same protocol as ALG-MA.

Methacryloyl (MA) functionalities were introduced to GEL through the widely used biphasic reaction with MAA. Initially, 1 g of GEL was dissolved in 10 mL of phosphate-buffered saline (PBS) at pH=7.4 and 50°C. Upon complete dissolution of the solid, 0.65 mL (4.4 mmol) of MAA was added dropwise under vigorous stirring (300 rpm). The reaction was maintained at 50°C for 2 hours, keeping the pH between 7 and 7.5 by adding diluted NaOH solution. Thus, GEL-MA was obtained, and the resulting mixture was diluted in 90 mL of deionized water and dialyzed against deionized water for four days to purify the methacrylated biopolymer. The dialysate water was changed after 2 hours and then every 12 hours. Finally, the purified product was freeze-dried and stored at −20°C until further use.

The degree of functionalization of carboxylate groups in ALG-MA and CS-MA, and free amino groups (lysine segments) in GEL-MA, were respectively 27 %, 50 %, and near to 100 % as determined by ^{1}H NMR spectroscopy. ^{1}H NMR spectra of the biopolymers before and after chemical modification can be found in the Supporting Information (Figure S1). The photocrosslinking of the methacrylated biopolymers was carried out with 5 mg mL^{-1} of PI in the inks and bioink formulations. The covalent photocrosslinking was made after inotropic crosslinking of the different hydrogels using a 100 mM $CaCl_2$ solution, employing a Blak-Ray UV lamp (Ted Pella, USA) with a wavelength of 365 nm and intensity of 9 mW cm^{-2} for 5 min (at 20 cm of distance) for the 3D printed scaffolds and a 3D bioprinter-incorporated UV head by illuminating the constructs with 365 nm light for 5 seconds with an intensity of 480 mW cm^{-2} (at ~ 2.8 cm of distance) during the bioprinting process.

GO nanoparticles were synthesized from graphite powder using a modified Hummers' method.[41] Initially, graphite powder (1.0 g) and sodium nitrate (0.5 g) were mixed, followed by the addition of 25 mL of concentrated sulfuric acid under constant stirring. After 30 minutes, $KMnO_4$ (3.0 g) was gradually added to

the above solution while maintaining the temperature below 20°C with an ice bath. The mixture was stirred at 35°C for 2 hours, and the resulting solution was diluted by adding 500 mL of water under vigorous stirring for 1 hour. The suspension was further treated with a 30% H_2O_2 solution (5 mL) to ensure the completion of the reaction of the $KMnO_4$ oxidant. The resulting mixture was centrifuged and washed with HCl and H_2O, respectively, followed by filtration. The solid residue was resuspended in deionized water, mechanically exfoliated for 1 hour using a Vibra-Cell Ultrasonic Processors VC 505 (Sonics & Materials), and freeze-dried in an Alpha 1-2 LSCbasic freeze-dryer (Martin Christ, Germany) to obtain few-layer GO sheets.

For a detailed characterization of the methacrylated biopolymers (ALG-MA, CS-MA, and GEL-MA) and GO, the reader is referred to the Supporting Information and our previous work.[23] The formulations of the inks used in scaffold 3D printing and the bioink used in construct 3D bioprinting are shown in Table 1.

2.2.2. Fabrication of scaffolds and constructs

As reported, the scaffolds were fabricated through 3D printing using a microextrusion method and maintained long-term in lyophilized form at -20 °C.[23] The 3D printing was carried out in a 4th generation 3D Bioplotter™ (Envisiontec, Germany) using polyethylene cartridges of 30 mL (Optimum® Components, Nordson EFD, USA) filled with the inks. The 3D printing conditions are detailed in the Supporting Information. For the biological evaluation, the freeze-dried 3D printed scaffolds (using an Alpha 1-2 LSCbasic freeze-dryer, Martin Christ, Germany) were cut to a circular form using a biopsy punch with a 7 mm diameter, a grid pattern with a width strand of ~500 µm, and strand separation of 1.5 mm. Before the cell

Table 1. Composition of inks and bioink

Formulation	ALG (mg mL^{-1})	ALG-MA (mg mL^{-1})	CS-MA (mg mL^{-1})	GEL-MA (mg mL^{-1})	GO (mg mL^{-1})	PI (mg mL^{-1})	FBS (% v/v)	hADMSCs (cells mL^{-1})
ACG	10.0	6.0	6.0	6.0	0	0.5	0	0
ACG/GO0.1	10.0	6.0	6.0	6.0	0.1	0.5	0	0
ACG/GO1.0	10.0	6.0	6.0	6.0	1.0	0.5	0	0
BIO- ACG/GO0.1	17.0	10.0	10.0	10.0	0.1	0.5	10	1×10^6

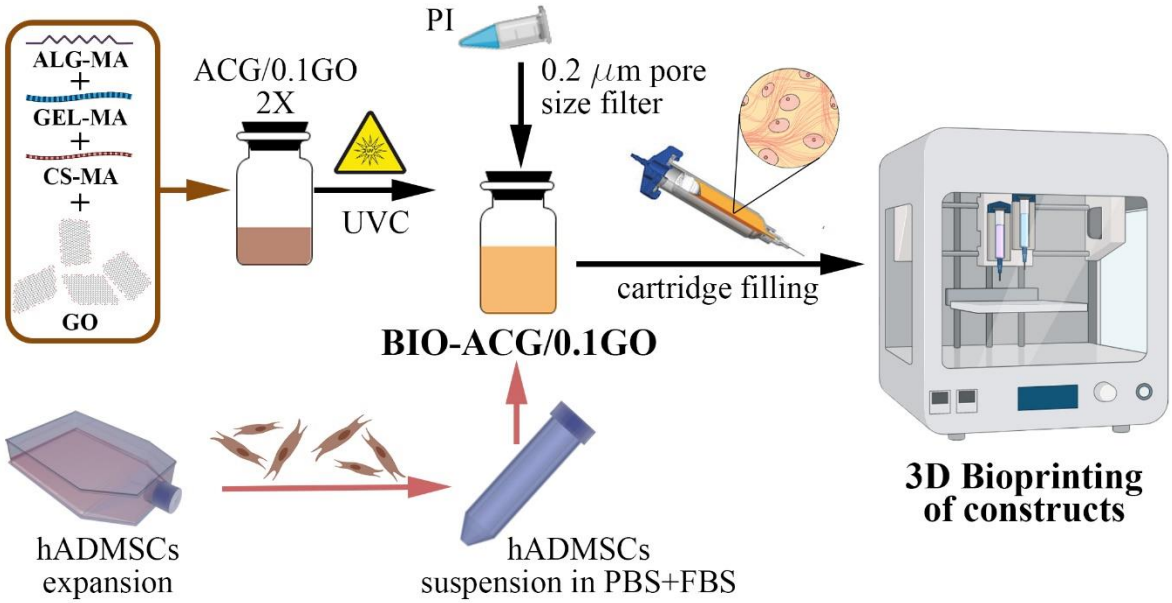

Figure 1. Schematic representation of the bioink formulation for the 3D bioprinting process.

seeding onto the scaffold, pre-conditioning with a conditioned culture medium (CCM) was necessary to rehydrate the lyophilized hydrogels. The swelling ratio of the formulation without GO (ACG) is 6, while in the formulations with GO, this parameter increases to about 10; as for the compressive elastic modulus, it is 60 kPa for ACG and approximately 100 kPa in hydrogels containing GO.[23] These values are consistent with the found in the literature for ALG/GEL hydrogels.[42]

The bioink components were sterilized with UV-C radiation for one hour, except for the PI stock solution, which was sterilized by filtration through a 0.22 µm filter. The biopolymers were gently dissolved in PBS (instead of pure water). This solution was mixed with aliquots of GO 5 mg mL^{-1}, PI 10 mg mL^{-1}, and hADMSCs suspended in fetal bovine serum (FBS, GE Healthcare, USA) to reach the concentrations described in Table 1. Figure 1 shows a general scheme of bioink preparation and 3D bioprinting. The constructs were fabricated on a 3DDiscovery™ Evolution bioprinter (regenHU, Switzerland). First, a 3 mL polyethylene cartridge (Optimum® Components, Nordson EFD, USA) is filled with the bioink under sterile conditions (between 1 and 3 mL, according to the need of constructs for subsequent assays) and kept at 5 °C for one

hour using a temperature control jacket on the print head. Construct printing is performed by microextrusion of the bioink through a 25 G needle into 6-well ultra-low attachment culture plates (Corning, USA). The bioprinting parameters were 1.5-2.0 bar of pressure and 30-35 mm s^{-1} of bioprinting speed. Once the first layer is printed, the construct is sprayed with a 100 mM $CaCl_2$ solution contained in a polyethylene cartridge coupled to an electromagnetic microvalve (inkjet head) to dispense a jet of the solution onto the printed layer. After the bioprinting of the construct is completed, the methacryloyl-modified biopolymers are photocrosslinked with a UV head by illuminating the constructs with 365 nm light for 5 seconds (480 mW cm^{-2} at ~ 2.8 cm). Finally, the excess crosslinking solution is removed by aspiration (after 5 min), a non-chondrogenic CCM is added, and the culture plates are placed in an incubator at 37 °C with a 5% CO_2 atmosphere.

2.2.3. Microscopy characterization

Field emission scanning electron microscopy (FESEM) images were acquired with an FEI Quanta™ FEG SEM electron microscope (USA). Transmission electron microscopy (TEM) images were acquired with an FEI Tecnai F20 S/TEM electron microscope (USA), mounting the sample on a Holey Carbon on a 300 mesh copper grid (Electron Microscopy Sciences, USA). Cell culture imaging was performed using a Leica DM IL LED phase contrast/inverted fluorescence microscope and a Leica MZ16F fluorescence stereomicroscope (Leica Microsystems, Germany). Both instruments had a Leica MC170 HD digital camera for microphotography acquisition (Leica Microsystems, Germany).

2.2.4. Cell culture and viability

The hADMSCs employed in this research were provided by the Texas A&M Health Science Center College of Medicine Institute for Regenerative Medicine at Scott & White (NIH Grant P40RR017447). Without further characterization, the cells were used for 3D bioprinting, live/dead assay, immunofluorescence analysis, and gene expression study. Following the provider's protocol, cells were expanded at low seeding densities (150 cells/cm^2) in CCM composed of Minimum Essential Medium Alpha (MEMα, Invitrogen, USA) supplemented

with 2 mM L-glutamine (Invitrogen, USA), 100 U/mL penicillin (Invitrogen, USA), 100 U/mL streptomycin (Invitrogen, USA), and 10% FBS (GE Healthcare, USA). Cells were maintained at 37 °C in an atmosphere of 5% CO_2. During expansion, the medium was refreshed every three days.

The in vitro cell survival in constructs was studied by Live/Dead assay with calcein-AM (Invitrogen) for the live cells staining and propidium iodide (Invitrogen, USA) for the dead cells staining. Live/Dead staining of hADMSCs into constructs was performed until day 21, after being washed with Dulbecco's phosphate saline buffer (DPBS, Invitrogen). For this, constructs were incubated in calcein-AM 5 mM/propidium iodine 5 mM in DPBS for 20 minutes at 37 °C and 5% CO_2 atmosphere. Following incubation, the samples were washed with DPBS and observed with a fluorescence stereomicroscope. Quantitative analysis of cell viability was performed by analysis of fluorescence images using ImageJ. The microphotographs acquired under the same conditions (exposure time, gain, aperture, etc.) in the green and red channels were processed to separate the RGB channels and measure the areas associated with the green (live cells) and red (dead cells) pixels to determine cell viability in percentage terms.

2.2.5. Immunofluorescence analysis

The immunofluorescence staining of chondrogenic markers for COLL II, ACAN, and SOX 9 was performed for hADMSCs (passage 9, 40000 cells/scaffold) cultured on 3D printed scaffolds and 3D bioprinted constructs after 28 days in CCM. Immunostaining was carried out as follows: scaffolds and constructs were washed twice in PBS at 37 °C, fixed in 4% paraformaldehyde (Electron Microscopy Sciences, USA) for 10 min, and washed twice in PBS. The hADMSCs of scaffolds and constructs were permeabilized with Triton X-100 (Sigma-Aldrich) 0.25 % in PBS-Gly (15 g glycine/100 mL PBS, Sigma-Aldrich) for 10 min, and then they were washed thrice in PBS-Gly. Cell-laden scaffolds and constructs were treated with blocking buffer (6% bovine serum albumin in PBS-Gly, Sigma-Aldrich) for 45 min and incubated overnight at 4 °C in rabbit polyclonal antibody against COLL II (ab34712, 1/100), ACAN (ab36861, 1/100), or SOX 9 (ab3697, 1:100) (Abcam, UK). After washing them three times in PBS-Gly, the scaffolds and constructs were then incubated in a secondary

antibody (1/100, Alexa Fluor 488 goat anti-rabbit IgG H&L ab150077, Abcam, UK) for 1 h at room temperature. Nuclei and F actin were counterstained using DAPI (4',6-diamidino-2-phenylindole) and TRITC-phalloidin (Life Technologies, USA), respectively. Cytoskeletal actin filaments were stained with TRITC-phalloidin at 1/200 dilution (300 units mL^{-1}) in PBS-Gly and incubated for 30 min at room temperature, followed by PBS-Gly washing. Next, nuclei staining was carried out by incubation for 10 min at room temperature with DAPI 2 μg mL^{-1} in PBS-Gly, followed by PBS-Gly washing. Finally, the samples were analyzed by fluorescence microscopy.

2.2.6. Quantification of gene expression

The gene expression of the chondrogenic marker type II collagen (COL2A1), SOX 9, aggrecan (ACAN), and the fibrillar protein type I collagen (COL1A1) was quantified by qRT-PCR. Cells-seeded scaffolds and cells-embedded constructs were washed with PBS and stored at −20 °C in RLT lysis buffer containing 1% β-mercaptoethanol. A Qiagen RNeasy® Plus Mini Kit (74134, Qiagen, Germany) was used to purify RNA from samples following the provider's protocol. RNA purity and concentration were determined using a NanoDrop ND-1000 spectrophotometer (Thermo Scientific, USA). Following the provider's protocol, RNA was converted into cDNA employing an RT2 First Strand Kit (330404, Qiagen, Germany). The synthesized cDNA was mixed with an RT2 SYBR Green ROX qPCR Mastermix (330524, Qiagen, Germany) and primer mix according to the supplier's protocol. Primers of human beta-actin (ACTB; Qiagen, Cod. PPH00073G-200 201708080124) as the housekeeping gene, human COL1A1 (Merck, Forward Cod. SY181118860-070 8812221733-000010 HA12359033-001, Reverse Cod. SY181118860-071 8812221733-000020 HA12359034-001)), human COL2A1 (Merck, Forward Cod. SY181118860-072 8812221733-000030 HA12359035-001, Reverse Cod. SY181118860-073 8812221733-000040 HA12359036-001), human SOX 9 (Merck, Forward Cod. SY181118860-076 8812221733-000090 HA12359041-001, Reverse Cod. SY181118860-077 8812221733-000100 HA12359042-001), and human ACAN (Merck, Forward Cod. SY181118860-078 8812221733-000110 HA12359043-001, Reverse Cod. SY181118860-079 8812221733-000120 HA12359044-001) were tested (primers' sequences are detailed in Table S1 of Supporting Information). Human XpressRef Universal Total

RNA (Qiagen, Germany) was used as a positive and interplate control. qRT-PCR was carried out in a StepOnePlus Real-Time PCR System instrument (Applied Biosystems, USA) under the following conditions: 10 min at 95 °C followed by 40 cycles of 15 s at 95 °C and 1 min at 60 °C. Finally, a melting curve was performed, having plates 15 s at 95 °C followed by 1 min at 60 °C and the melting step from 60 to 95 °C. Relative gene-fold variations were determined by the $2^{-\Delta\Delta Ct}$ method using ACTB as the housekeeping gene and compared to a control sample of hADMSCs cultured in a 2D plastic dish with CCM. Three samples were measured per condition (n = 3).

2.2.7. Statistical analysis

The analysis of variance (ANOVA) and Tukey's post-test were performed to assess the statistical significance between groups using Prism 6 (GraphPad).

3. Results and Discussion

3.1. 3D bioprinting

Before 3D bioprinting, 3D-printed scaffolds were fabricated based on our previous work for complementary material characterization. First, the ink-loaded cartridge (~ 10 mL of ink) was placed in the print head at 5 °C, inducing the thermotropic pre-gelation of the GEL chains. Then, the scaffolds were printed by micro-extrusion onto a Petri dish with a 100 mM calcium chloride solution to produce an ionotropic crosslinking of ALG and ALG-MA chains. The printing platform was adjusted to 2 °C to promote, in parallel, the thermotropic gelation of the gelatin component in ACG, ACG/GO0.1, and ACG/GO1.0 inks. When a few design layers were printed, additional calcium(II) crosslinking solution was sprayed on these layers to ensure ionotropic crosslinking. The full-crosslinking time for these inks is about 4 minutes, according to a previously reported kinetic analysis by rheology.[23] Therefore, the 3D printed scaffolds were kept in contact with the crosslinking solution for 5 min. The finished 3D-printed scaffolds were irradiated with UV light to perform the secondary covalent crosslinking (bioconjugation) of methacryloyl groups present in ALG-MA, CS-MA, and GEL-MA.

The chemical nature of the 3D-printed (freeze-dried) scaffolds was analyzed by FTIR spectroscopy. Figure 2a-c shows the ATR-FTIR spectra of the three scaffold compositions (ACG, ACG/GO0.1, and ACG/GO1.0, respectively) together with the spectra of the individual methacrylated biopolymers and GO. The chemical modification of ALG with methacryloyl groups produces a shoulder in the carbonyl stretching band of the ALG structure above 1715 cm^{-1} (red line spectrum in Figure 2a-c). After the photocrosslinking reaction, this shoulder disappears because of the band shift to lower energy (black line spectrum in Figure 2a-c). An intense broad band is observed around 1630 cm^{-1} in the ACG/GO0.1 sample, resulting from overlapping the stretching mode vibrations of C=O bonds of the carbonyls present in the biopolymers and GO, in addition to the C=C stretching of aromatic structures present in the gelatin and GO (black line spectrum in Figure 2b). A higher GO concentration increments the interaction by hydrogen bonds, as the energy of the C=O band is shifted from 1715 cm^{-1} to 1630 cm^{-1} (black line spectrum in Figure 2c). Hydrogen bonds also are evidenced because of the blue-shifted amide II vibration of GEL-MA (1534 cm^{-1}) in ACG (8 cm^{-1}), ACG/0.1GO (16 cm^{-1}), and ACG/1.0GO (21 cm^{-1}). The formation of hydrogen bonding with GO results in better thixotropic properties of the inks and, consequently, in higher printing quality through the action of GO nanoparticles as a physical crosslinker via this hydrogen bonding.[23,43]

In previous work, the cytocompatibility of the materials employed in this study was evaluated by supporting hADMSCs on 3D-printed scaffolds.[23] The cytocompatibility of such hydrogels is due in part to the bioconjugation of alginate with gelatin and natural components of the ECM, which increases the adhesion and proliferation of different cell phenotypes, including MSCs.[42,44,45] These results showed further that scaffolds with low GO concentrations exhibited both higher cell proliferation and better cell distribution

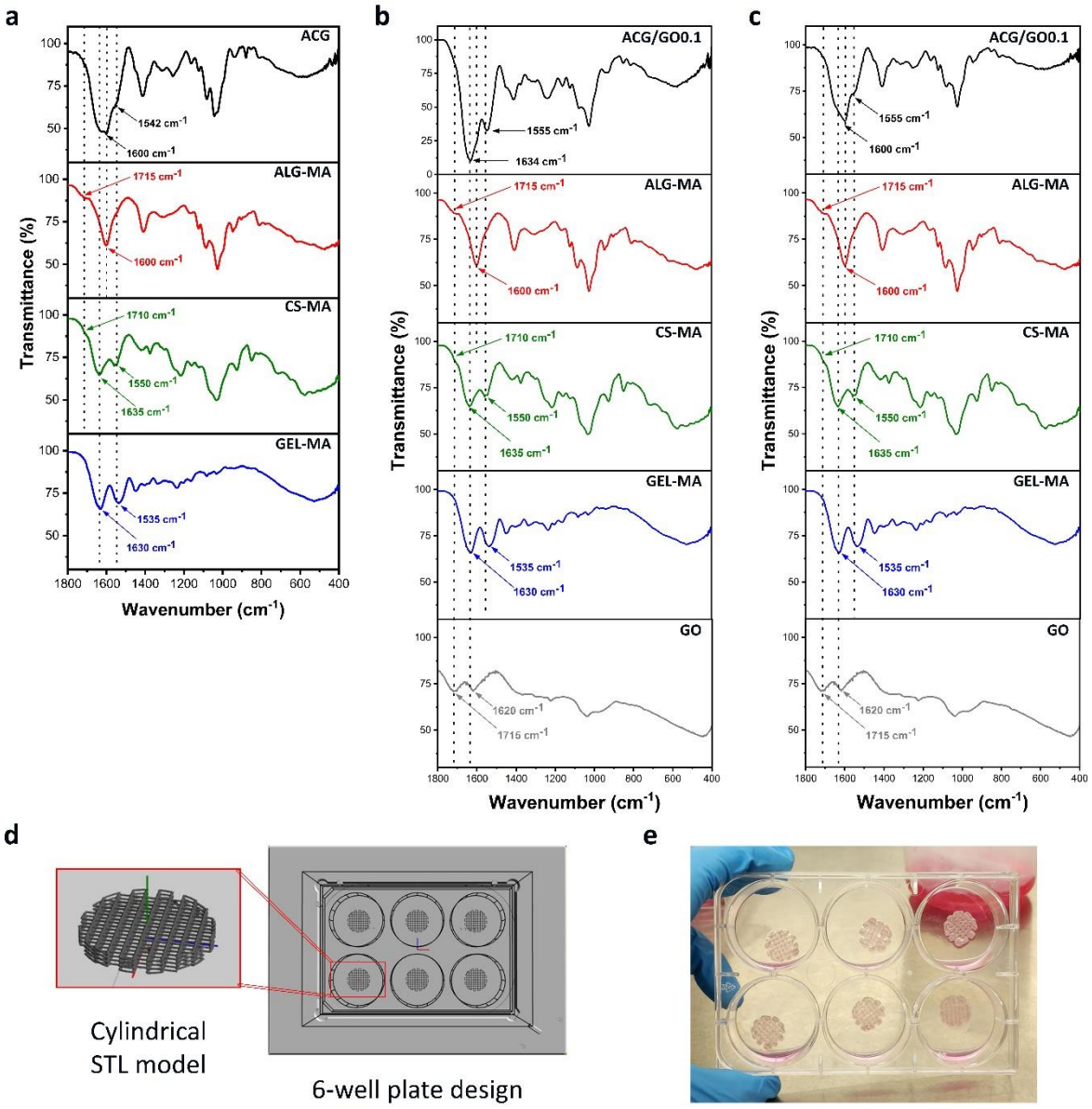

Figure 2. ATR-FTIR spectra of (a) ACG, (b) ACG/GO0.1, and (c) ACG/GO1.0 scaffolds. The spectra of ALG-MA, CS-MA, GEL-MA, and GO are shown in red, green, blue, and grey, respectively. (d) Computer-aided design (CAD) of a grid-like cylindrical model of constructs placed in a 6-well culture plate. (e) 3D bioprinted constructs in a 6-well plate after one day in CCM.

than scaffolds based on pure hydrogel and composite with high GO concentration, as concluded through fluorescent staining and alamarBlue™ assays. The formulation for the bioink was, therefore, based on the sample with the highest biological performance in 3D printing: ACG/GO0.1 ink,[23] which further agrees with

the optimal GO concentration (0.1 mg mL^{-1}) from other contributions.[39] Compared to the original ACG/GO0.1 formulation, the concentration of all biopolymers in BIO-ACG/GO0.1 bioink was increased to compensate for viscosity reduction because of the cells and FBS incorporation. Regarding the rheological properties of this type of formulation based on ALG, GEL, CS, and GO, the hydrogels exhibit non-Newtonian shear-thinning fluid behavior.[23] This behavior is common in alginate and other biopolymer hydrogels for 3D printing applications.[44,45] Furthermore, these formulations exhibit thixotropic behavior during the microextrusion process when passing through the printer needle, which is determinant in the shape fidelity of the 3D printed structures.[43,45] As demonstrated in our previous work, the incorporation of GO in the formulations decreases the viscosity recovery time after the hydrogel is extruded, improving the printing quality of the scaffolds or constructs.[23]

Before bioprinting, the BIO-ACG/GO0.1 bioink in the cartridge was kept at 5 °C for one hour to both thermotropically pre-gelling the GEL-MA chains present and keep the hADMSCs with minimal metabolic activity to avoid cell stressing. [46] The 3D bioprinting process starts with printing two layers of the designed structure on the bottom of a well, followed by applying a $CaCl_2$ solution over the printed layers for ionotropic crosslinking between calcium cations and ALG and ALG-MA chains. This primary crosslinking is fast enough to maintain the constructs' shape fidelity and structural integrity. Finally, the construct is irradiated with a UV LED lamp to conduct the bioconjugation through the methacrylated biopolymers' photocrosslinking (Video S1 in Supporting Information). Figure S2a-c shows a two-layer construct at different magnifications after the bioprinting process. The constructs presented well-defined strands that allowed the building of the desired mesh-like structure. In particular, the formulated bioink allowed the bioprinting of 0.5 mm width strands able to manufacture cylindrical constructs of 15 mm diameter with a total height of 0.5 mm (after two layers, meaning 0.25 mm per layer), having 2 mm strand spacing, designed in BioCAD™ software in 6-well culture plates (Figure 2d-e). It also allowed printing forms as small as 10 mm in diameter by 0.8 mm and 2.2 mm high cylinders (4 and 12 printed layers, respectively), as shown in Figure S2d-f. Two-layer bioprinted constructs were used for subsequent biological evaluations.

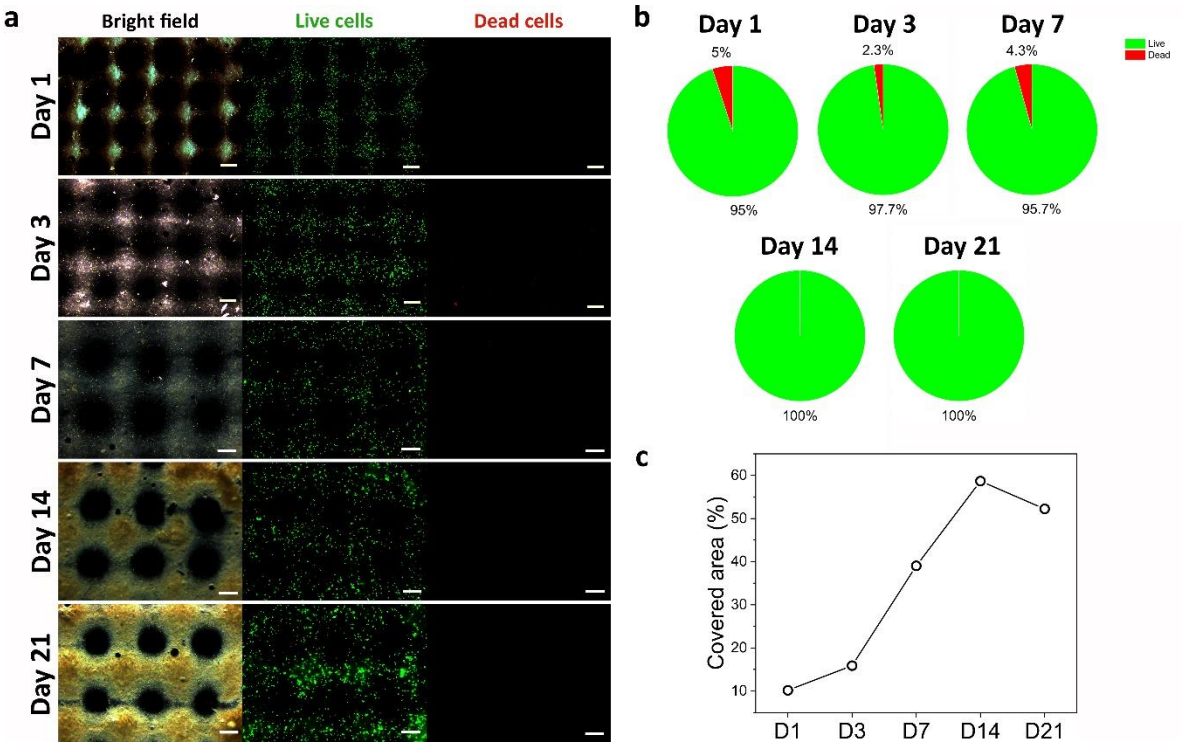

Figure 3. (a) Fluorescence stereomicroscopy images of Live/Dead assay of 3D bioprinted constructs at different time points (scale bar: 600 µm). (b) Cell viability in 3D bioprinted constructs at different time points. (c) Variation of the area covered by the construct, which is expressed as a percentage of the visual field in the microphotographs.

The survival of hADMSCs, embedded into BIO-ACG/GO0.1 bioink, after the 3D bioprinting process was studied by fluorescence microscopy through Live/Dead assay. High cell viability (predominantly green-stained cells) up to day 21 of culture in CCM was observed with a homogeneous cell distribution, as shown in Figure 3a (negative control for red-stained dead cells is shown in Figure S3a). Taking into account that the main disadvantages of extrusion-based bioprinting are the moderate cell viability rate (40-80 %) and the relatively low printing speed,[47] our results are outstanding as the constructs were printed with a high cell density (~1 × 10^6 hADMSCs mL^{-1}) and at a speed of up to 35 mm s^{-1} (limit of the equipment used), maintaining cell viability close to 100 % during several weeks of in vitro culture, as shown in Figure 3b. Moreover, after 21 days of culture, the constructs exhibit a progressive thickening of their strands (bright field images in Figure 3a), which could be associated with the production of ECM by the embedded cells.

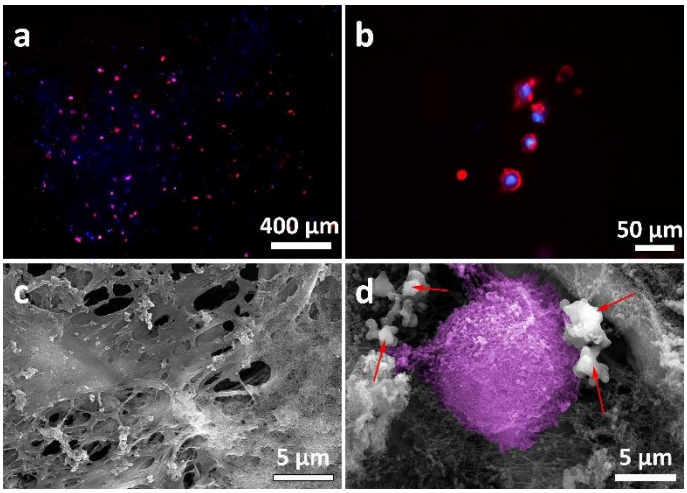

Figure 4. Fluorescence microscopy images of (a) 3D-bioprinted cells displaying the cell distribution and (b) cell morphology in the BIO-ACG/GO0.1 bioink. Actin filaments in the cytoskeleton are stained red, and nuclei in blue. FESEM images of the construct (c) without cells and (d) with cells, where it is possible to observe the interaction between a cell (purple) and the biomaterial (protein aggregates are shown with red arrows).

After two weeks of in vitro culture, the area covered by the construct increases from 10% (day 1) to over 50%, which is maintained until day 21 (Figure 3c).

Figure 4a-b shows representative fluorescence microscopy images of hADMSCs (passage 10) in the 3D bioprinted constructs on day 3 of culture in CCM. The low-magnification micrographs (Figure 4a) reveal a homogeneous distribution of cells within the bioprinted construct. Figure 4b shows the spheroid cell structure, where the nucleus (blue) surrounded by the cytoskeleton (red) is visible. The spherical morphology of embedded cells in BIO-ACG/GO0.1 agrees with the shape of chondrocytes in their natural niche.[48] Representative FESEM images of ethanol-dehydrated (concentration gradient method) 3D-bioprinted samples show that the polymeric matrix displayed a porous tridimensional microstructure (Figure 4c) and that the hADMSCs (purple) are able to interact with the biopolymeric matrix (grayscale) in the bioink(Figure 4d). Spherical aggregates around the cell are further observed, which could be associated with proteins secreted by the cell itself or from the fetal bovine serum used as a supplement in the formulation of the bioink and the culture medium (red arrows in Figure 4d).

3.2. Immunofluorescence staining

Immunofluorescence staining was performed to study the effect of GO composition and processing by characterizing the chondrogenic differentiation of hADMSCs on 3D-printed scaffolds and into 3D-bioprinted constructs. The chondrogenic markers COLL II (extracellular matrix produced by chondrocytes), ACAN (extracellular matrix produced by chondrocytes), and SOX 9 (transcription factor during chondrocyte differentiation) were analyzed.[49] Figure 5 shows fluorescence images of the different 3D-printed materials seeded with hADMSCs and the cell-embedded bioink, observed after 35 days of culture in CCM without chondrogenic supplementation. Cell viability at day 35 was checked by Live/Dead assay, as shown in Figure S3b. In Figure 5, immunofluorescence staining is shown in green for all chondrogenic markers, and counterstaining of phalloidin and DAPI was used to indicate the location of cytoskeleton F-actin and cell nuclei (red and blue, respectively). Positive staining for COLL II, ACAN, and SOX 9 antigens were found in the three printed scaffolds (ACG, ACG/GO0.1, and ACG/GO1.0), as well as in the bioprinted BIO-ACG/GO0.1

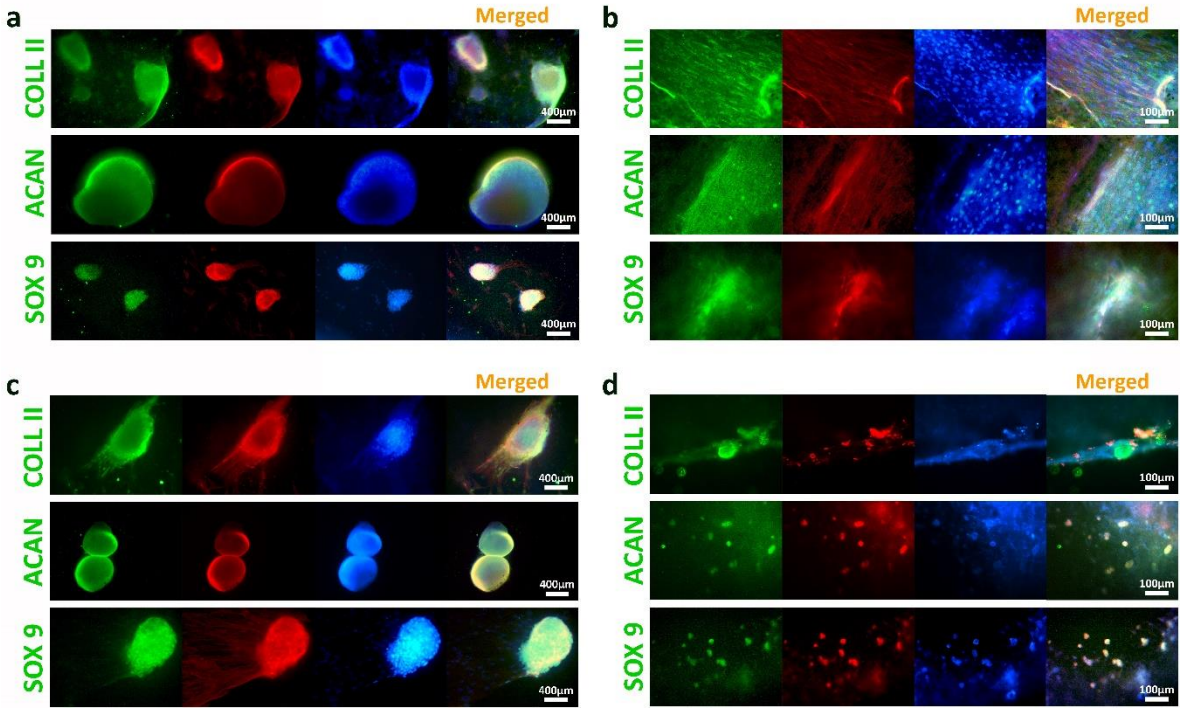

Figure 5. Immunofluorescence images of the chondrogenic markers (green) present in (a) 3D-printed ACG, (b) ACG/GO0.1, (c) ACG/GO1.0 scaffolds, and (d) 3D-bioprinted BIO-ACG/GO0.1 construct at day 35. Actin filaments in the cytoskeleton are stained red, and nuclei in blue.

constructs, meaning that all the 3D-printed formulations have the capacity of intrinsically induce a chondrogenic effect on hADMSCs and that the bioprinting process did not affect this differentiation characteristic.

For 3D printed samples, high cell density aggregates were observed in the scaffolds' surface without GO and with high GO concentration (ACG and ACG/GO1.0, respectively, Figure 5 a and c). In contrast, the scaffolds with GO at low concentrations (ACG/GO0.1) markedly improve cell distribution and ECM deposition (i.e., COLL II and ACAN) on the 3D printed scaffolds, exhibiting homogeneous and aligned cell proliferation over the scaffold strands, macropores and around the scaffold edges (Figure 5b).

The immunofluorescence study performed on the bioprinted constructs also shows the secretion of chondrogenic markers (Figure 5d), although with a lower amount of analyte than the 3D-printed scaffolds, probably because of the lower cell density and limited cell mobility within the bioprinted strands. Nevertheless, after 35 days of culture in CCM, the production of COLL II, ACAN, and SOX 9 was observed in the extra- and intracellular environment. Thus, BIO-ACG/GO0.1 bioink and the subsequent extrusion during bioprinting do not affect the chondroinductive characteristics of the biomimetic hydrogel. In addition, the morphology of cells and distribution into BIO-ACG/GO0.1 seem to replicate the native cartilage structure.

Considering that the strategy usually employed to induce chondrogenic differentiation involves using a culture medium supplemented with a biochemical cocktail, our results confirm that this approach can be avoided by designing biomimicking hydrogels.[50–52] Noteworthy, our results show that our biomimetic approach is valid not only for 3D printing but also for 3D bioprinting processes.

3.3. Chondrogenic gene expression

For a quantitative comparison of the effect of GO and the processing in the chondroinductive properties of the developed biomaterials, the gene expression of chondrogenic markers was studied by RT-qPCR to the cells cultured on the 3D-printed scaffolds and 3D-bioprinted constructs using non-chondrogenic medium (CCM). Figure 6a shows the fold-change of gene expression of markers associated with the secretion of type II collagen (COL2A1), aggrecan (ACAN), and SOX 9 for the different 3D-printed scaffolds and 3D-bioprinted

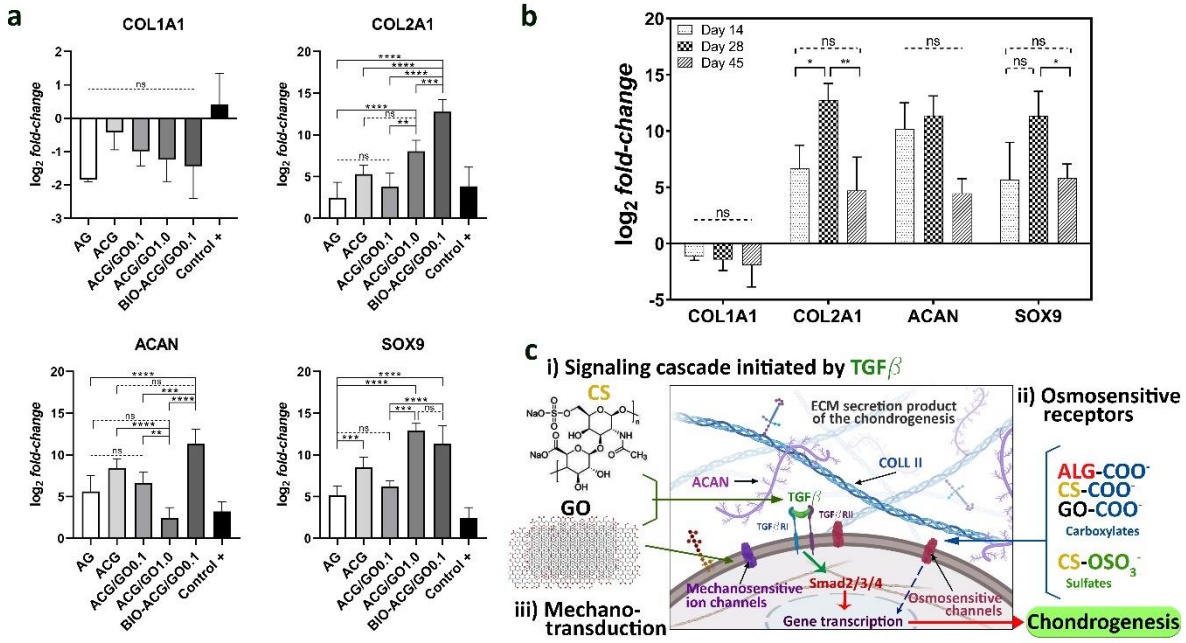

Figure 6. (a) Gene expression analysis by RT-qPCR of markers associated with the secretion of type I collagen (COL1A1), type II collagen (COL2A1), aggrecan (ACAN), and SOX 9 in the cells cultured on the scaffolds and constructs using a non-chondrogenic medium at day 28. (b) Effect of time on the chondrogenesis process in BIO-ACG/GO0.1. (c) Possible mechanisms of induced chondrogenesis on hADMSCs by the developed biomaterial: i) Signaling cascade initiated y TGF-β and modulated by the CS and GO present in the formulation (Smad2/3/4: a family of proteins that are the main signal transducers for receptors of the TGF-β superfamily), ii) Hyperosmolarity-induced pathway because of negatively charged groups of the polysaccharides and GO, and iii) Mechanotransduction pathway because of the increase in cell membrane tension by interaction with GO.

construct after 28 days of culture. The hADMSCs cultured on a polystyrene plate (2D culture) were used as a reference. A 3D-printed scaffold using a hydrogel based on ALG bioconjugated with GEL (AG) was further analyzed to compare with ACG scaffolds and elucidate the ability of CS to act as an intrinsically chondroinductive biomaterial. In addition to the chondrogenic markers, the gene expression associated with type I collagen (COL1A1) production was analyzed to assess neocartilage fibrillation. Independent of the chemical composition of the biomaterials tested and the 3D printing process, COL1A1 gene expression was negative relative to the 2D culture control hADMSCs (Figure 6a). Downregulation of COL1A1 indicates that

the process of chondrogenic differentiation occurs without dedifferentiation and does not follow an undesired fibrillar tissue (fibrocartilage) formation pathway.[53]

The downregulation of COL1A1 markers occurred with an upregulation of the gene expression of the chondrogenic markers in all 3D-printed formulations and bioprinted construct, which is in agreement with the immunofluorescence results shown above. These results confirm that the formulations are intrinsically chondroinductive on hADMSCs. Regarding the effect of CS, the positive gene expression of COL2A1 and ACAN in AG and ACG scaffolds showed no significant statistical difference (Figure 6a), indicating that CS is not needed for stimulating cartilage ECM secretion in vitro in these formulations and that ALG bioconjugated only with GEL can do it. However, the gene expression of the transcription marker SOX 9 was significantly higher in ACG scaffolds compared to AG scaffolds, showing that incorporating CS into the scaffolds promotes chondrogenic differentiation since this type of GAG can modulate the activity of growth factors secreted by cells during chondrogenesis.[54]

The gene expression of COL2A1 and SOX 9 was significantly higher in ACG/GO1.0 scaffolds (Figure 6a), evidencing a coadjuvant effect of a high concentration of GO in the COLL II deposition and the cell differentiation process. The ACAN gene expression was significantly lower in ACG/GO1.0 than in the rest of the scaffolds analyzed, which would indicate an inhibitory effect of GO at high concentrations on the secretion of this glycoprotein at late stages (28 days) or that the maximum of ACAN gene expression was reached at a time before or after the analysis. A recent work studying the effect of GO on chondrogenic differentiation of MSCs in poly(D-L-lactic acid)/poly(ethylene glycol) based hydrogel nanocomposites demonstrated the chondroinductive capacity of GO in the absence of chondroinductive growth factors.[55] This study suggests that the chondroinductive effect of GO may arise from the sequestering ability of chondrogenic signaling, which increases the local concentration of pro-chondrogenic stimuli. On the other hand, the increase in negative charges due to the carboxylate groups of GO could increase osmolarity (hyperosmolarity), favoring chondrogenesis.[56]

The intrinsically chondroinductive capacity of the ACG/GO hydrogel is also observed in 3D-bioprinted constructs, as concluded by results from RT-qPCR analysis (Figure 6a). Noteworthy, the cells embedded into BIO-ACG/GO0.1 constructs had a significantly larger expression of chondrogenic genes than those supported on the 3D-printed ACG/GO0.1 scaffolds. This behavior could be attributable to a higher biopolymer concentration and the cell's morphology and distribution into BIO-ACG/GO0.1, which simulate the cartilage organization.

Considering the best performance of bioprinted constructs and their high potential for the next generation of therapies based on biomimetic materials, the effect of time on the gene expression levels of chondrogenic markers was further analyzed (between days 14 and 45 post-bioprinting). Figure 6b shows that although all three chondrogenic markers were positively expressed after 14 days of culture of the bioprinted constructs in CCM, there was a significant effect of the time elapsed as the relative expression peaked at day 28. Noteworthy, the results correspond with the time window in MSC-engineered tissues when chondrogenic differentiation reaches a plateau and neocartilage is formed in culture media supplemented with chondrogenic biochemical agents.[57,58] This result confirms that the biomimetic hydrogel can replicate even the chondrogenesis times in the cell dynamic.

The study of the chondroinductive properties of the developed biomaterials shows that biomimicking the chemical composition of the ECM plays a key role in the material's bioactivity in 3D printing/bioprinting. While the bioconjugated hydrogel, ACG, showed biocompatibility and intrinsically chondrogenic characteristics, the processability as a 3D printing ink is limited compared to nanocomposites with GO because of differences in their rheological properties.[23] In addition, GO at low concentrations prevented the formation of large cell aggregates, such as those observed in the ACG formulation. Incorporating GO in the scaffolds improved cell adhesion and distribution in the early stages of culture and increased the chondrogenic capacity of the biomaterial. Furthermore, the performance of GO is concentration-dependent since although ACG/GO1.0 scaffolds exhibited better chondrogenic performance, the formation of cell aggregates in late culture stages makes the ACG/GO0.1 formulation a better choice in scaffold fabrication.

The bioactivity of GO in these nanocomposites as an adjuvant in the process of proliferation and chondrogenesis may be due to both the ability to adsorb growth factors, proteins, and nutrients in a localized manner, as well as the increased negative charge density that increases osmolarity. The formulation of the ACG/GO0.1 ink and the BIO-ACG/GO0.1 bioink of homologous composition (same ALG:SC:GEL ratio plus 0.1 mg mL^{-1} of GO) present an optimal balance between processability for obtaining 3D-printed scaffolds and 3D-bioprinted constructs, as well as bioactivity and cellular distribution.

Figure 6c shows a schematic representation of three possible mechanisms explaining the chondrogenic process of hADMSCs on the biomimetic nanocomposited hydrogels. On one pathway, the CS can bind to the hADMSCs by molecular docking with calcium-sensing receptors that increase the intracellular calcium ion level (promoted by the calcium-rich environment from crosslinking cations), stimulating the secretion of TGF-β.[59] The increase of TGF-β can induces chondrogenesis via the Smad-dependent signaling pathway.[60] First, TGF-β interact with the type II receptor (TGF-β RII), activating the type I receptor (TGF-β RI) that induces the phosphorylation of R-Smads (Smad2, 3) and Co-Smad (Smad4) transfer into the nucleus. Then, Smads signal transducers regulate the gene expression of SOX9 downstream, which in turn triggers the gene transcription process that results in the chondrogenic differentiation of hADMSCs. Other non-Smad-dependent pathways include mitogen-activated protein kinase (MAPK), Wnt signaling, and Notch signaling.[60] The hyperosmotic microenvironment stimulates osmosensitive receptors that induce chondrogenesis because of the highly negatively charged material components in the second mechanism pathway. In particular, the tonicity-responsive enhancer-binding protein (TonEBP) is a transcriptional regulator of the cellular response to hypertonic stress that regulates the expression of osmoprotective genes involved in the osmoadaption of chondrogenic MSCs.[61] Consequently, chondrogenic differentiation stimulates the secretion of the cartilage's own ECM to generate new tissue. The GO nanoparticles also have a relevant function in the mechanism's pathway mentioned above since their adsorption feature could help to increase the localized availability of cell-secreted cytokines (e.g., TGF-β). Furthermore, the chemical structure of GO is rich in negatively charged carboxylate groups that can activate the osmosensitive receptor on cells.

Recent work by Ogene et al. has contributed to clarifying the possible mechanisms of action of GO in the chondrogenic process.[62] This research has found that a canonical activation occurs through GO-induced Smad 2 phosphorylation, indicating TGF-β signaling. In addition, this work also evidenced the activation of a third possible chondrogenic pathway mediated by mechanosensitive ion channels due to a GO-mediated increase in cell membrane tension. As a consequence of this phenomenon, the action of GO particles activates endogenous latent TGF-β, intrinsically inducing chondrogenic differentiation. Based on the results of this work, CS and GO in the nanocomposite hydrogels can synergically promote chondrogenesis on hADMSCs.

4. Conclusions

This work presents a biomimetic nanocomposited hydrogel for developing 3D printed scaffolds and 3D bioprinting constructs. The material is based on alginate bioconjugated covalently crosslinked with gelatin and chondroitin sulfate through the methacrylation of pure biopolymers, using graphene oxide as filler in the nanocomposite hydrogel. Based on this nanocomposite, three different formulations were used to evaluate the bioactivity of 3D-printed scaffolds in terms of chondroinductivity. The bioconjugated scaffolds showed cytocompatibility with hADMSCs in vitro, and the samples with GO exhibited outstanding cell proliferation and distribution on the scaffolds. A novel nanocomposite formulation with 0.1 mg mL^{-1} of GO was further used in combination with hADMSCs to perform 3D bioprinting of constructs, exhibiting extraordinary long-term cell viability and shape fidelity. Immunofluorescence analysis and gene expression study indicate that the bioconjugated alginate polymeric matrix is intrinsically chondroinductive on the differentiation of hADMSCs in 3D-printed scaffolds and 3D-bioprinted constructs without the need to use a culture medium with pro-chondrogenesis agents and factors. The addition of GO enhances chondrogenic differentiation, thus promoting neocartilage formation. Notably, the chondroinductive nature of nanocomposite hydrogel is enhanced in 3D-bioprinted constructs with embedded cells. According to gene expression analysis, 0.1 mg mL^{-1} of GO is an adequate concentration to improve the chondrogenesis on hADMSCs. These results are relevant since the development of intrinsically chondroinductive biomaterials

has been barely reported. 3D bioprinting of BIO-ACG/GO0.1 constructs can potentially become a structural and biologically functional tool for CTE applications.

ASSOCIATED CONTENT

Supporting Information.

The Supporting Information is available free of charge on the ACS Publications website at DOI: 10.1021/xxxxxx.

^{1}H NMR characterization of used pure commercial and methacrylated biopolymers. Electronic microscopy images showing the morphology of the synthesized GO. Fabrication of 3D-printed scaffolds. Primer sequences used in qRT-PCR. Optical microscope images of the 3D bioprinted constructs. Stereomicroscopy image of negative control for Live/Dead assay and Live/Dead assay on day 35 of a culture of the 3D bioprinted constructs (PDF). Video showing the 3D bioprinting process (MP4).

Acknowledgments

The authors thank the financial support of ANID under FONDEQUIP Projects EQM150101 and EQM140012 and project ANID-Basal Center of Interventional Medicine for Precision and Advanced Cellular Therapy, IMPACT, # FB210024. F.O.-M. thanks to ANID (ex CONICYT) Beca de Doctorado Nacional 21150039 and FONDECYT de Postdoctorado 3240135. TOC graphic created using BioRender.

References

(1) Guo, J. L.; Kim, Y. S.; Mikos, A. G. Biomacromolecules for Tissue Engineering: Emerging Biomimetic Strategies. *Biomacromolecules* **2019**, *20* (8), 2904–2912. https://doi.org/10.1021/acs.biomac.9b00792.

(2) Costantini, M.; Idaszek, J.; Szöke, K.; Jaroszewicz, J.; Dentini, M.; Barbetta, A.; Brinchmann, J. E.; Święszkowski, W. 3D Bioprinting of BM-MSCs-Loaded ECM Biomimetic Hydrogels for in Vitro Neocartilage Formation. *Biofabrication* **2016**, *8* (3), 035002. https://doi.org/10.1088/1758-

5090/8/3/035002.

(3) Ngadimin, K. D.; Stokes, A.; Gentile, P.; Ferreira, A. M. Biomimetic Hydrogels Designed for Cartilage Tissue Engineering. *Biomater. Sci.* **2021**, *9* (12), 4246–4259. https://doi.org/10.1039/d0bm01852j.

(4) Nasiri, N.; Hosseini, S.; Alini, M.; Khademhosseini, A.; Baghaban Eslaminejad, M. Targeted Cell Delivery for Articular Cartilage Regeneration and Osteoarthritis Treatment. *Drug Discov. Today* **2019**, *24* (11), 2212–2224. https://doi.org/10.1016/j.drudis.2019.07.010.

(5) Tonti, O. R.; Larson, H.; Lipp, S. N.; Luetkemeyer, C. M.; Makam, M.; Vargas, D.; Wilcox, S. M.; Calve, S. Tissue-Specific Parameters for the Design of ECM-Mimetic Biomaterials. *Acta Biomater.* **2021**, *132*, 83–102. https://doi.org/10.1016/j.actbio.2021.04.017.

(6) Afewerki, S.; Sheikhi, A.; Kannan, S.; Ahadian, S.; Khademhosseini, A. Gelatin-Polysaccharide Composite Scaffolds for 3D Cell Culture and Tissue Engineering: Towards Natural Therapeutics. *Bioeng. Transl. Med.* **2019**, *4* (1), 96–115. https://doi.org/10.1002/btm2.10124.

(7) Hölzl, K.; Fürsatz, M.; Göcerler, H.; Schädl, B.; Žigon-Branc, S.; Markovic, M.; Gahleitner, C.; Hoorick, J. Van; Van Vlierberghe, S.; Kleiner, A.; et al. Gelatin Methacryloyl as Environment for Chondrocytes and Cell Delivery to Superficial Cartilage Defects. *J. Tissue Eng. Regen. Med.* **2022**, *16* (2), 207–222. https://doi.org/10.1002/term.3273.

(8) Davidenko, N.; Schuster, C. F.; Bax, D. V.; Farndale, R. W.; Hamaia, S.; Best, S. M.; Cameron, R. E. Evaluation of Cell Binding to Collagen and Gelatin: A Study of the Effect of 2D and 3D Architecture and Surface Chemistry. *J. Mater. Sci. Mater. Med.* **2016**, *27* (10), 148. https://doi.org/10.1007/s10856-016-5763-9.

(9) Yang, J.; Shen, M.; Wen, H.; Luo, Y.; Huang, R.; Rong, L.; Xie, J. Recent Advance in Delivery System and Tissue Engineering Applications of Chondroitin Sulfate. *Carbohydr. Polym.* **2020**, *230* (235), 115650. https://doi.org/10.1016/j.carbpol.2019.115650.

(10) Kiani, C.; Chen, L.; Wu, Y. J.; Yee, A. J.; Yang, B. B. Structure and Function of Aggrecan. *Cell Res.* **2002**, *12* (1), 19–32. https://doi.org/10.1038/sj.cr.7290106.

(11) Hayes, A. J.; Melrose, J. Aggrecan, the Primary Weight-Bearing Cartilage Proteoglycan, Has Context-Dependent, Cell-Directive Properties in Embryonic Development and Neurogenesis: Aggrecan Glycan Side Chain Modifications Convey Interactive Biodiversity. *Biomolecules* **2020**, *10* (9), 1244. https://doi.org/10.3390/biom10091244.

(12) Menezes, R.; Vincent, R.; Osorno, L.; Hu, P.; Arinzeh, T. L. Biomaterials and Tissue Engineering Approaches Using Glycosaminoglycans for Tissue Repair: Lessons Learned from the Native Extracellular Matrix. *Acta Biomater.* **2023**, *163*, 210–227. https://doi.org/10.1016/j.actbio.2022.09.064.

(13) Bauza-Mayol, G.; Quintela, M.; Brozovich, A.; Hopson, M.; Shaikh, S.; Cabrera, F.; Shi, A.; Niclot, F. B.; Paradiso, F.; Combellack, E.; et al. Biomimetic Scaffolds Modulate the Posttraumatic Inflammatory Response in Articular Cartilage Contributing to Enhanced Neoformation of Cartilaginous Tissue In Vivo. *Adv. Healthc. Mater.* **2022**, *11* (1), 1–18. https://doi.org/10.1002/adhm.202101127.

(14) Vassallo, V.; Tsianaka, A.; Alessio, N.; Grübel, J.; Cammarota, M.; Tovar, G. E. M.; Southan, A.; Schiraldi, C. Evaluation of Novel Biomaterials for Cartilage Regeneration Based on Gelatin Methacryloyl Interpenetrated with Extractive Chondroitin Sulfate or Unsulfated Biotechnological Chondroitin. *J. Biomed. Mater. Res. - Part A* **2022**, *110* (6), 1210–1223. https://doi.org/10.1002/jbm.a.37364.

(15) Honarpardaz, A.; Irani, S.; Pezeshki-Modaress, M.; Zandi, M.; Sadeghi, A. Enhanced Chondrogenic Differentiation of Bone Marrow Mesenchymal Stem Cells on Gelatin/Glycosaminoglycan Electrospun Nanofibers with Different Amount of Glycosaminoglycan. *J. Biomed. Mater. Res. - Part A* **2019**, *107* (1), 38–48. https://doi.org/10.1002/jbm.a.36501.

(16) Shin, J.; Kang, E. H.; Choi, S.; Jeon, E. J.; Cho, J. H.; Kang, D.; Lee, H.; Yun, I. S.; Cho, S. W. Tissue-

Adhesive Chondroitin Sulfate Hydrogel for Cartilage Reconstruction. *ACS Biomater. Sci. Eng.* **2021**, *7* (9), 4230–4243. https://doi.org/10.1021/acsbiomaterials.0c01414.

(17) Rubí-Sans, G.; Recha-Sancho, L.; Pérez-Amodio, S.; Mateos-Timoneda, M. Á.; Semino, C. E.; Engel, E. Development of a Three-Dimensional Bioengineered Platform for Articular Cartilage Regeneration. *Biomolecules* **2019**, *10* (1), 52. https://doi.org/10.3390/biom10010052.

(18) Robert, A. W.; Marcon, B. H.; Dallagiovanna, B.; Shigunov, P. Adipogenesis, Osteogenesis, and Chondrogenesis of Human Mesenchymal Stem/Stromal Cells: A Comparative Transcriptome Approach. *Front. Cell Dev. Biol.* **2020**, *8* (July), 561. https://doi.org/10.3389/fcell.2020.00561.

(19) Hesari, R.; Keshvarinia, M.; Kabiri, M.; Rad, I.; Parivar, K.; Hoseinpoor, H.; Tavakoli, R.; Soleimani, M.; Kouhkan, F.; Zamanluee, S.; et al. Comparative Impact of Platelet Rich Plasma and Transforming Growth Factor-β on Chondrogenic Differentiation of Human Adipose Derived Stem Cells. *BioImpacts* **2020**, *10* (1), 37–43. https://doi.org/10.15171/bi.2020.05.

(20) Drabsch, Y.; Ten Dijke, P. TGF-β Signalling and Its Role in Cancer Progression and Metastasis. *Cancer Metastasis Rev.* **2012**, *31* (3–4), 553–568. https://doi.org/10.1007/s10555-012-9375-7.

(21) Zhu, M.; Zhong, W.; Cao, W.; Zhang, Q.; Wu, G. Chondroinductive/Chondroconductive Peptides and Their-Functionalized Biomaterials for Cartilage Tissue Engineering. *Bioact. Mater.* **2022**, *9* (May 2021), 221–238. https://doi.org/10.1016/j.bioactmat.2021.07.004.

(22) Sutherland, A. J.; Beck, E. C.; Dennis, S. C.; Converse, G. L.; Hopkins, R. A.; Berkland, C. J.; Detamore, M. S. Decellularized Cartilage May Be a Chondroinductive Material for Osteochondral Tissue Engineering. *PLoS One* **2015**, *10* (5), 1–13. https://doi.org/10.1371/journal.pone.0121966.

(23) Olate-Moya, F.; Arens, L.; Wilhelm, M.; Mateos-Timoneda, M. A.; Engel, E.; Palza, H. Chondroinductive Alginate-Based Hydrogels Having Graphene Oxide for 3D Printed Scaffold Fabrication. *ACS Appl. Mater. Interfaces* **2020**, *12* (4), 4343–4357.

https://doi.org/10.1021/acsami.9b22062.

(24) Stamnitz, S.; Klimczak, A. Mesenchymal Stem Cells, Bioactive Factors, and Scaffolds in Bone Repair: From Research Perspectives to Clinical Practice. *Cells* **2021**, *10* (8), 1925. https://doi.org/10.3390/cells10081925.

(25) Irani, S.; Honarpardaz, A.; Choubini, N.; Pezeshki-Modaress, M.; Zandi, M. Chondro-Inductive Nanofibrous Scaffold Based Gelatin/Polyvinyl Alcohol/Chondroitin Sulfate for Cartilage Tissue Engineering. *Polym. Adv. Technol.* **2020**, *31* (6), 1395–1402. https://doi.org/10.1002/pat.4869.

(26) Sharifi, F.; Irani, S.; Azadegan, G.; Pezeshki-Modaress, M.; Zandi, M.; Saeed, M. Co-Electrospun Gelatin-Chondroitin Sulfate/Polycaprolactone Nanofibrous Scaffolds for Cartilage Tissue Engineering. *Bioact. Carbohydrates Diet. Fibre* **2020**, *22* (March), 100215. https://doi.org/10.1016/j.bcdf.2020.100215.

(27) Kudaibergen, G.; Zhunussova, M.; Mun, E. A.; Ramankulov, Y.; Ogay, V. Macroporous Cell-Laden Gelatin/Hyaluronic Acid/Chondroitin Sulfate Cryogels for Engineered Tissue Constructs. *Gels* **2022**, *8* (9), 590. https://doi.org/10.3390/gels8090590.

(28) Meghdadi, M.; Pezeshki-Modaress, M.; Irani, S.; Atyabi, S. M.; Zandi, M. Chondroitin Sulfate Immobilized PCL Nanofibers Enhance Chondrogenic Differentiation of Mesenchymal Stem Cells. *Int. J. Biol. Macromol.* **2019**, *136*, 616–624. https://doi.org/10.1016/j.ijbiomac.2019.06.061.

(29) Varma, M. V.; Kandasubramanian, B.; Ibrahim, S. M. 3D Printed Scaffolds for Biomedical Applications. *Mater. Chem. Phys.* **2020**, *255* (August), 123642. https://doi.org/10.1016/j.matchemphys.2020.123642.

(30) Schwab, A.; Levato, R.; D'Este, M.; Piluso, S.; Eglin, D.; Malda, J. Printability and Shape Fidelity of Bioinks in 3D Bioprinting. *Chem. Rev.* **2020**, *120* (19), 11028–11055. https://doi.org/10.1021/acs.chemrev.0c00084.

(31) Murphy, S. V.; De Coppi, P.; Atala, A. Opportunities and Challenges of Translational 3D Bioprinting. *Nat. Biomed. Eng.* **2020**, *4* (4), 370–380. https://doi.org/10.1038/s41551-019-0471-7.

(32) Decante, G.; Costa, J. B.; Silva-Correia, J.; Collins, M. N.; Reis, R. L.; Oliveira, J. M. Engineering Bioinks for 3D Bioprinting. *Biofabrication* **2021**, *13* (3), 032001. https://doi.org/10.1088/1758-5090/abec2c.

(33) Axpe, E.; Oyen, M. Applications of Alginate-Based Bioinks in 3D Bioprinting. *Int. J. Mol. Sci.* **2016**, *17* (12), 1976. https://doi.org/10.3390/ijms17121976.

(34) Hull, S. M.; Brunel, L. G.; Heilshorn, S. C. 3D Bioprinting of Cell-Laden Hydrogels for Improved Biological Functionality. *Adv. Mater.* **2022**, *34* (2), 1–17. https://doi.org/10.1002/adma.202103691.

(35) Islam, M.; Lantada, A. D.; Mager, D.; Korvink, J. G. Carbon-Based Materials for Articular Tissue Engineering: From Innovative Scaffolding Materials toward Engineered Living Carbon. *Adv. Healthc. Mater.* **2022**, *11* (1), 1–25. https://doi.org/10.1002/adhm.202101834.

(36) Liu, H.; Chen, J.; Qiao, S.; Zhang, W. Carbon-Based Nanomaterials for Bone and Cartilage Regeneration: A Review. *ACS Biomater. Sci. Eng.* **2021**, *7* (10), 4718–4735. https://doi.org/10.1021/acsbiomaterials.1c00759.

(37) Rastin, H.; Mansouri, N.; Tung, T. T.; Hassan, K.; Mazinani, A.; Ramezanpour, M.; Yap, P. L.; Yu, L.; Vreugde, S.; Losic, D. Converging 2D Nanomaterials and 3D Bioprinting Technology: State-of-the-Art, Challenges, and Potential Outlook in Biomedical Applications. *Adv. Healthc. Mater.* **2021**, *10* (22), e2101439. https://doi.org/10.1002/adhm.202101439.

(38) Qi, X.; Jiang, F.; Zhou, M.; Zhang, W.; Jiang, X. Graphene Oxide as a Promising Material in Dentistry and Tissue Regeneration: A Review. *Smart Mater. Med.* **2021**, *2* (July), 280–291. https://doi.org/10.1016/j.smaim.2021.08.001.

(39) Zhou, X.; Nowicki, M.; Cui, H.; Zhu, W.; Fang, X.; Miao, S.; Lee, S. J.; Keidar, M.; Zhang, L. G. 3D Bioprinted Graphene Oxide-Incorporated Matrix for Promoting Chondrogenic Differentiation of

Human Bone Marrow Mesenchymal Stem Cells. *Carbon N. Y.* **2017**, *116*, 615–624. https://doi.org/10.1016/j.carbon.2017.02.049.

(40) García-Lizarribar, A.; Fernández-Garibay, X.; Velasco-Mallorquí, F.; Castaño, A. G.; Samitier, J.; Ramon-Azcon, J. Composite Biomaterials as Long-Lasting Scaffolds for 3D Bioprinting of Highly Aligned Muscle Tissue. *Macromol. Biosci.* **2018**, *1800167*, 1–13. https://doi.org/10.1002/mabi.201800167.

(41) Olate-Moya, F.; Palza, H. Effect of Graphene Oxide on the PH-responsive Drug Release from Supramolecular Hydrogels. *J. Appl. Polym. Sci.* **2022**, *139* (1), 51420. https://doi.org/10.1002/app.51420.

(42) Serafin, A.; Culebras, M.; Collins, M. N. Synthesis and Evaluation of Alginate, Gelatin, and Hyaluronic Acid Hybrid Hydrogels for Tissue Engineering Applications. *Int. J. Biol. Macromol.* **2023**, *233* (January), 123438. https://doi.org/10.1016/j.ijbiomac.2023.123438.

(43) Li, H.; Liu, S.; Lin, L. Rheological Study on 3D Printability of Alginate Hydrogel and Effect of Graphene Oxide. *Int. J. Bioprinting* **2016**, *2* (2), 54–66. https://doi.org/10.18063/IJB.2016.02.007.

(44) Zamboni, F.; Ren, G.; Culebras, M.; O'Driscoll, J.; O'Dwyer, J.; Ryan, E. J.; Collins, M. N. Curcumin Encapsulated Polylactic Acid Nanoparticles Embedded in Alginate/Gelatin Bioinks for in Situ Immunoregulation: Characterization and Biological Assessment. *Int. J. Biol. Macromol.* **2022**, *221* (May), 1218–1227. https://doi.org/10.1016/j.ijbiomac.2022.09.014.

(45) Serafin, A.; Culebras, M.; Oliveira, J. M.; Koffler, J.; Collins, M. N. 3D Printable Electroconductive Gelatin-Hyaluronic Acid Materials Containing Polypyrrole Nanoparticles for Electroactive Tissue Engineering. *Adv. Compos. Hybrid Mater.* **2023**, *6* (3), 109. https://doi.org/10.1007/s42114-023-00665-w.

(46) Muraki, K.; Hirose, M.; Kotobuki, N.; Kato, Y.; Machida, H.; Takakura, Y.; Ohgushi, H. Assessment of

Viability and Osteogenic Ability of Human Mesenchymal Stem Cells After Being Stored in Suspension for Clinical Transplantation. *Tissue Eng.* **2006**, *0* (0), 060706073730041. https://doi.org/10.1089/ten.2006.12.ft-122.

(47) Heinrich, M. A.; Liu, W.; Jimenez, A.; Yang, J.; Akpek, A.; Liu, X.; Pi, Q.; Mu, X.; Hu, N.; Schiffelers, R. M.; et al. 3D Bioprinting: From Benches to Translational Applications. *Small* **2019**, *1805510*, 1805510. https://doi.org/10.1002/smll.201805510.

(48) Karim, A.; Amin, A. K.; Hall, A. C. The Clustering and Morphology of Chondrocytes in Normal and Mildly Degenerate Human Femoral Head Cartilage Studied by Confocal Laser Scanning Microscopy. *J. Anat.* **2018**, *232* (4), 686–698. https://doi.org/10.1111/joa.12768.

(49) Han, S.; Li, Y.; Chan, B. P. Extracellular Protease Inhibition Alters the Phenotype of Chondrogenically Differentiating Human Mesenchymal Stem Cells (MSCs) in 3D Collagen Microspheres. *PLoS One* **2016**, *11* (1), 1–14. https://doi.org/10.1371/journal.pone.0146928.

(50) Zhu, W.; Cui, H.; Boualam, B.; Masood, F.; Flynn, E.; Rao, R. D.; Zhang, Z.-Y.; Zhang, L. G. 3D Bioprinting Mesenchymal Stem Cell-Laden Construct with Core–Shell Nanospheres for Cartilage Tissue Engineering. *Nanotechnology* **2018**, *29* (18), 185101. https://doi.org/10.1088/1361-6528/aaafa1.

(51) Rathan, S.; Dejob, L.; Schipani, R.; Haffner, B.; Möbius, M. E.; Kelly, D. J. Fiber Reinforced Cartilage ECM Functionalized Bioinks for Functional Cartilage Tissue Engineering. *Adv. Healthc. Mater.* **2019**, *8* (7), 1801501. https://doi.org/10.1002/adhm.201801501.

(52) Zhu, D.; Tong, X.; Trinh, P.; Yang, F. Mimicking Cartilage Tissue Zonal Organization by Engineering Tissue-Scale Gradient Hydrogels as 3D Cell Niche. *Tissue Eng. Part A* **2017**, *24* (1–2), 1–10. https://doi.org/10.1089/ten.tea.2016.0453.

(53) Li, X.; Teng, Y.; Liu, J.; Lin, H.; Fan, Y.; Zhang, X. Chondrogenic Differentiation of BMSCs Encapsulated

in Chondroinductive Polysaccharide/Collagen Hybrid Hydrogels. *J. Mater. Chem. B* **2017**, *5* (26), 5109–5119. https://doi.org/10.1039/c7tb01020f.

(54) Knudson, C. B. Hyaluronan and CD44: Strategic Players for Cell-Matrix Interactions during Chondrogenesis and Matrix Assembly. *Birth Defects Res. Part C - Embryo Today Rev.* **2003**, *69* (2), 174–196. https://doi.org/10.1002/bdrc.10013.

(55) Shen, H.; Lin, H.; Sun, A. X.; Song, S.; Zhang, Z.; Dai, J.; Tuan, R. S. Chondroinductive Factor-Free Chondrogenic Differentiation of Human Mesenchymal Stem Cells in Graphene Oxide-Incorporated Hydrogels. *J. Mater. Chem. B* **2018**, *6* (6), 908–917. https://doi.org/10.1039/C7TB02172K.

(56) Alliston, T. Chondroitin Sulfate and Growth Factor Signaling in the Skeleton: Possible Links to MPS VI. *J. Pediatr. Rehabil. Med.* **2010**, *3* (2), 129–138. https://doi.org/10.3233/PRM-2010-0117.

(57) Gadjanski, I.; Spiller, K.; Vunjak-Novakovic, G. Time-Dependent Processes in Stem Cell-Based Tissue Engineering of Articular Cartilage. *Stem Cell Rev. Reports* **2012**, *8* (3), 863–881. https://doi.org/10.1007/s12015-011-9328-5.

(58) Xu, J.; Wang, W.; Ludeman, M.; Cheng, K.; Hayami, T.; Lotz, J. C.; Kapila, S. Chondrogenic Differentiation of Human Mesenchymal Stem Cells in Three-Dimensional Alginate Gels. *Tissue Eng. - Part A.* **2008**, *14* (5), 667–680. https://doi.org/10.1089/tea.2007.0272.

(59) Shen, Q.; Zhang, C.; Mo, H.; Zhang, H.; Qin, X.; Li, J.; Zhang, Z.; Richel, A. Fabrication of Chondroitin Sulfate Calcium Complex and Its Chondrocyte Proliferation in Vitro. *Carbohydr. Polym.* **2021**, *254* (August 2020), 117282. https://doi.org/10.1016/j.carbpol.2020.117282.

(60) Chen, H.; Tan, X. N.; Hu, S.; Liu, R. Q.; Peng, L. H.; Li, Y. M.; Wu, P. Molecular Mechanisms of Chondrocyte Proliferation and Differentiation. *Front. Cell Dev. Biol.* **2021**, *9* (May), 1–13. https://doi.org/10.3389/fcell.2021.664168.

(61) Ahmadyan, S.; Kabiri, M.; Hanaee-Ahvaz, H.; Farazmand, A. Osmolyte Type and the Osmolarity Level

Affect Chondrogenesis of Mesenchymal Stem Cells. *Appl. Biochem. Biotechnol.* **2018**, *185* (2), 507–523. https://doi.org/10.1007/s12010-017-2647-5.

(62) Ogene, L.; Woods, S.; Hetmanski, J.; Lozano, N.; Karakasidi, A.; Caswell, P. T.; Kostarelos, K.; Domingos, M. A. N.; Vranic, S.; Kimber, S. J. Graphene Oxide Activates Canonical TGFβ Signalling in a Human Chondrocyte Cell Line via Increased Plasma Membrane Tension. *Nanoscale* **2024**, *16* (11), 5653–5664. https://doi.org/10.1039/D3NR06033K.

Figure 1. Schematic representation of the bioink formulation for the 3D bioprinting process.

Figure 2. ATR-FTIR spectra of (a) ACG, (b) ACG/GO0.1, and (c) ACG/GO1.0 scaffolds. The spectra of ALG-MA, CS-MA, GEL-MA, and GO are shown in red, green, blue, and grey, respectively. (d) Computer-aided design (CAD) of a grid-like cylindrical model of constructs placed in a 6-well culture plate. (e) 3D bioprinted constructs in a 6-well plate after one day in CCM.

Figure 3. (a) Fluorescence stereomicroscopy images of Live/Dead assay of 3D bioprinted constructs at different time points (scale bar: 600 µm). (b) Cell viability in 3D bioprinted constructs at different time points. (c) Variation of the area covered by the construct, which is expressed as a percentage of the visual field in the microphotographs.

Figure 4. Fluorescence microscopy images of (a) 3D-bioprinted cells displaying the cell distribution and (b) cell morphology in the BIO-ACG/GO0.1 bioink. Actin filaments in the cytoskeleton are stained red, and nuclei in blue. FESEM images of the construct (c) without cells and (d) with cells, where it is possible to observe the interaction between a cell (purple) and the biomaterial (protein aggregates are shown with red arrows).

Figure 5. Immunofluorescence images of the chondrogenic markers (green) present in (a) 3D-printed ACG, (b) ACG/GO0.1, (c) ACG/GO1.0 scaffolds, and (d) 3D-bioprinted BIO-ACG/GO0.1 construct at day 35. Actin filaments in the cytoskeleton are stained red, and nuclei in blue.

Figure 6. (a) Gene expression analysis by RT-qPCR of markers associated with the secretion of type I collagen (COL1A1), type II collagen (COL2A1), aggrecan (ACAN), and SOX 9 in the cells cultured on the scaffolds and constructs using a non-chondrogenic medium at day 28. (b) Effect of time on the chondrogenesis process in BIO-ACG/GO0.1. (c) Possible mechanisms of induced chondrogenesis on hADMSCs by the developed biomaterial: i) Signaling cascade initiated y TGF-β and modulated by the CS and GO present in the formulation (Smad2/3/4: a family of proteins that are the main signal transducers for receptors of the TGF-β superfamily), ii) Hyperosmolarity-induced pathway because of negatively charged groups of the polysaccharides and GO, and iii) Mechanotransduction pathway because of the increase in cell membrane tension by interaction with GO.

Table 1. Composition of inks and bioink

Formulation	ALG (mg mL^{-1})	ALG-MA (mg mL^{-1})	CS-MA (mg mL^{-1})	GEL-MA (mg mL^{-1})	GO (mg mL^{-1})	PI (mg mL^{-1})	FBS (% v/v)	hADMSCs (cells mL^{-1})
ACG	10.0	6.0	6.0	6.0	0	0.5	0	0
ACG/GO0.1	10.0	6.0	6.0	6.0	0.1	0.5	0	0
ACG/GO1.0	10.0	6.0	6.0	6.0	1.0	0.5	0	0
BIO- ACG/GO0.1	17.0	10.0	10.0	10.0	0.1	0.5	10	1×10^6

For Table of Contents Use Only

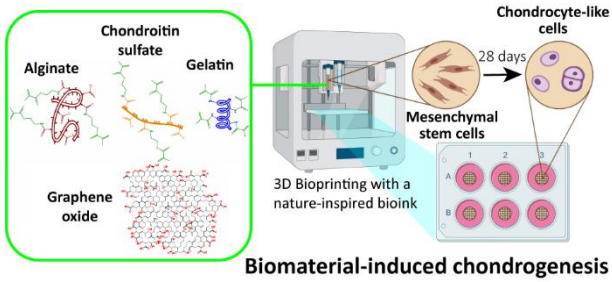

Biomaterial-induced chondrogenesis